

# CTForensics: A Comprehensive Dataset and Method for AI-Generated CT Image Detection

Yiheng Li<sup>1,2</sup>, Zichang Tan<sup>4</sup>, Guoqing Xu<sup>1,2</sup>, Yijun Ye<sup>1,2</sup>, Yang Yang<sup>1,2, (✉)</sup>,  
Zhen Lei<sup>1,2,3</sup>,

<sup>1</sup> School of Artificial Intelligence, University of Chinese Academy of Sciences

<sup>2</sup> MAIS, Institute of Automation, Chinese Academy of Sciences

<sup>3</sup> CAIR, HKISI, Chinese Academy of Sciences, <sup>4</sup> Sangfor Technologies Inc.

{liyiheng2024, yangyang2013, zhen.lei}@ia.ac.cn, tanzichang@foxmail.com

Repo: <https://github.com/liyih/CTForensics>

**Abstract.** With the rapid development of generative AI in medical imaging, synthetic Computed Tomography (CT) images have demonstrated great potential in applications such as data augmentation and clinical diagnosis, but they also introduce serious security risks. Despite the increasing security concerns, existing studies on CT forgery detection are still limited and fail to adequately address real-world challenges. These limitations are mainly reflected in two aspects: the absence of datasets that can effectively evaluate model generalization to reflect the real-world application requirements, and the reliance on detection methods designed for natural images that are insensitive to CT-specific forgery artifacts. In this view, we propose **CTForensics**, a comprehensive dataset designed to systematically evaluate the generalization capability of CT forgery detection methods, which includes ten diverse CT generative methods. Moreover, we introduce the **Enhanced Spatial-Frequency CT Forgery Detector (ESF-CTFD)**, an efficient CNN-based neural network that captures forgery cues across the wavelet, spatial, and frequency domains. First, it transforms the input CT image into three scales and extracts features at each scale via the Wavelet-Enhanced Central Stem. Then, starting from the largest-scale features, the Spatial Process Block gradually performs feature fusion with the smaller-scale ones. Finally, the Frequency Process Block learns frequency-domain information for predicting the final results. Experiments demonstrate that ESF-CTFD consistently outperforms existing methods and exhibits superior generalization across different CT generative models.

**Keywords:** CT · Forgery Detection · Generalization · Dataset

## 1 Introduction

In recent years, the rapid advancement of generative artificial intelligence (AI), particularly GANs [4] and diffusion models [23], has enabled the synthesis of highly realistic images. In the medical imaging domain, these models have been

increasingly adopted to generate synthetic data for tasks such as data augmentation and modality translation, with computed tomography (CT) being a prominent example. However, the high realism of AI-generated CT images raises critical concerns for clinical safety and data trustworthiness, since synthetic scans may be imperceptible to humans and automated systems, potentially leading to erroneous diagnoses. In this view, it is imperative to develop robust detection mechanisms capable of accurately distinguishing between authentic and AI-generated CT scans to safeguard the integrity of medical diagnostics.

Despite the urgent need for effective countermeasures, a primary obstacle in the field is the lack of a CT forgery dataset that truly reflects real-world application demands. Existing datasets [1,15] only contain fake CT scans from limited kinds of CT generative methods. To bridge this gap, we propose **CTForensics**, a comprehensive dataset comprising 4 GAN-based and 6 diffusion-based generation methods, for a total of 10 distinct generative models. Inspired by natural image forgery detection [20,26,14], this dataset focuses on evaluating model generalization to unseen generation methods. This is because generative techniques evolve rapidly in real-world clinical settings, and detection systems must be able to counter unpredictable algorithms. Without robust generalization, the security of medical diagnoses cannot be guaranteed.

Another significant challenge lies in the methodology. Existing forgery detection methods [20,26,14,25,16] are largely adapted from natural image analysis and often neglect the unique imaging mechanisms and physical characteristics of medical CT scans. In particular, CT images exhibit modality-specific noise distributions and statistical properties that are poorly captured by models focusing on RGB-domain texture artifacts, limiting their ability to detect subtle medical forgeries. To address this gap, we propose **ESF-CTFD**, a dedicated framework that synergistically exploits complementary forgery cues across spatial, frequency, and wavelet domains. It comprises of three components, i.e., Wavelet-Enhanced Central Stem (WCS), Spatial Process Block (SPB) and Frequency Process Block (FPB). WCS integrates wavelet decomposition and central correlation convolution to model local pixel relationships and enhance fine-grained forgery features. SPB preserves the anatomical structural consistency and spatial integrity of CT images during feature propagation. FPB explores the critical frequency-domain statistics and artifacts to amplify the subtle, imperceptible traces of forgeries that are difficult to identify in the spatial domain. Extensive experiments on the CTForensic dataset demonstrate that ESF-CTFD consistently outperforms state-of-the-art methods, achieving superior sensitivity and specificity in distinguishing authentic and AI-generated CT images.

## 2 Related Work

**CT Image Generation.** Recent advances in generative models have enabled the synthesis of realistic CT images for data augmentation and simulation. Some work [12,17] uses GAN-based [4] networks to synthesize CT images. For instance, CTGAN [18] injects or removes cancerous tumors using a conditional GAN. HA-

GAN [24] proposed an end-to-end architecture that can simultaneously generate a low-resolution version of an image and a randomly selected sub-volume from the high-resolution image. In contrast, some methods [10] adopt diffusion-based [23] architectures to generate CT images. Specifically, Lung-DDPM [9] generates high-fidelity CT images based on semantic layout-guided denoising diffusion probabilistic models. BTM [5] leverages the StableDiffusion model [22] to tamper the medical CT images. Recent methods [28] generate CT images based on medical language text prompts. For example, GenerateCT [6] generates CT images conditioned on medical text prompts using a causal vision transformer and a text-conditional super-resolution diffusion model. Text2CT [19] generates anatomically consistent 3D CT volumes from radiology text prompts using a latent diffusion model with 3D contrastive vision-language pretraining and a volumetric VAE.

**Forgery CT Detection.** To ensure the privacy and security of users, some work [21] has begun to focus on CT forgery detection. MedForensics [15] proposes a large-scale dataset that discusses six medical modalities, while BTM [5] introduces a diffusion-based anomaly detection method for medical images. However, both methods share a common limitation in that they do not systematically evaluate model generalization across diverse CT generative methods; specifically, the former considers only one generation approach [11], while the latter examines only two [18,22]. Most methods conduct a standard convolutional network [8] or their variants to extract discriminative features for CT forgery detection. For example, MedNet [1] proposes a customized EfficientNetV2-based [27] model with a spatial-channel attention mechanism to detect lung CT deepfakes.

### 3 Problem Definition

Given a CT image  $x \in \mathbb{R}^{C \times H \times W}$  and its corresponding label  $y \in Y = \{0, 1\}$ , the goal is to learn a classifier that can accurately map each input  $x$  to its true label  $y$ , effectively capturing subtle forgery artifacts. Here,  $y = 0$  indicates an authentic CT image and  $y = 1$  denotes a forged one.

In terms of task setting, we follow the widely adopted generalization paradigm in AI-generated image detection [20], where the model is trained using fake images from a single generative method, while being evaluated on multiple unseen forgery types at test time. This setting reflects real-world scenarios in which image generation techniques evolve continuously, and attackers may employ novel manipulation methods not present in the training data to evade detection.

### 4 The Proposed CTForensics Dataset

To evaluate the detection model’s ability to distinguish fake from real CT scans, we construct a new dataset, termed CTForensics, which is designed to reflect realistic and challenging CT image forgery scenarios. It contains a total of 75990 images, with half being real and the other half being fake. For the training set, the real images are sourced from the CT-RATE dataset [7], and we randomly extract

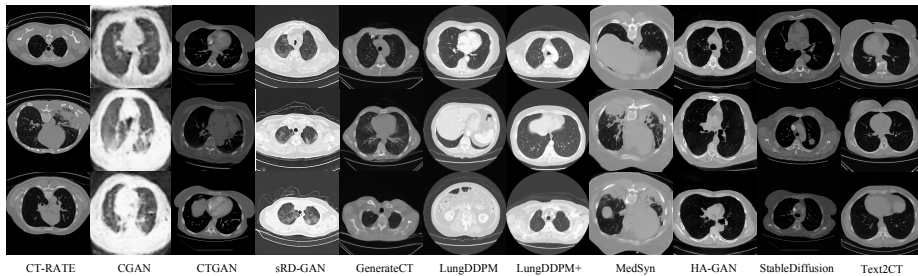


Fig. 1. Visualization of CTForensics Dataset.

23000 2D CT slices from the original 3D CT releases. Fake images are generated using HA-GAN [24], with an equal number of real and synthetic images.

For the testing set, we employ ten generative models for image generation, including CGAN [17], CTGAN [18], sRD-GAN [12], GenerateCT [6], LungDDPM [9], LungDDPM+ [10], MedSyn [28], HA-GAN [24], StableDiffusion [22], and Text2CT [19]. For CTGAN and StableDiffusion, the fake CT images are collected from the testing set of BTD [5]. For CGAN and sRD-GAN, fake CT images are obtained from their official releases. For Text2CT and GenerateCT, we collect their officially generated 3D CT volumes and randomly extract 2D slices as fake CT images. For LungDDPM, LungDDPM+, HA-GAN, and MedSyn, we deploy the models and generate fake CT images by inference using the official pre-trained weights. Additionally, for MedSyn, the generation prompts are sampled from radiology text reports in the CT-RATE dataset [7]. The real counterpart of each generative model is obtained from the CT-RATE dataset, with the number of real CT images matched to that of the corresponding synthetic samples to ensure a balanced evaluation. Examples of real and generated CT images are shown in Fig. 1, all of them are processed and saved as single-channel grayscale PNG images in further experiments. Additionally, we guarantee the quality of each image in the dataset via automated and manual reviews.

## 5 Method

### 5.1 Overview

As shown in Fig. 2 (a), the ESF-CTFD first resamples the original CT into three resolution scales, with a  $2\times$  down-sampling factor between every two adjacent scales. At each resolution scale, multi-scale initial feature maps are extracted through Wavelet-Enhanced Central Stem. The initial feature map with the highest resolution is further processed and downsampled through a Spatial Process Block, then fused with the medium-scale initial feature map. The resulting fused feature map passes through another Spatial Process Block before being fused with the smallest-scale feature map. Subsequently, the features are processed by a cascaded Frequency Process Block and ultimately utilized for final prediction.

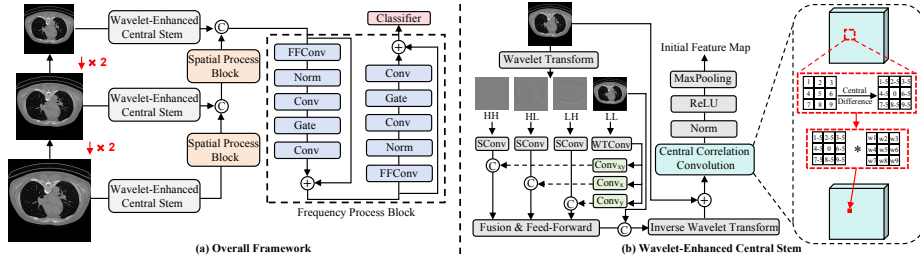


Fig. 2. Overall framework of our proposed ESF-CTFD.

## 5.2 Spatial-Wavelet Stem

As shown in Fig. 2 (b), given the input CT scan  $I \in R^{C \times H \times W}$ , wavelet transform is conducted to decompose it into four different frequency sub-bands:  $hh, hl, lh, ll \in R^{C \times \frac{H}{2} \times \frac{W}{2}}$ , where  $C$  is the number of input channels, while  $H$  and  $W$  denote the spatial height and width of the CT scan, respectively.  $hh, hl$  and  $lh$  sub-bands comprise more high-frequency information, whereas the  $ll$  sub-band is dominated by low-frequency components. In light of this property,  $hh, hl$ , and  $lh$  are processed by the Depth-wise Separable Convolutions (DSConv) with a smaller receptive field, while  $ll$  is handled by WTConv [3], which possesses a larger receptive field. Inspired by CWNNet [30], to further enhance the extraction of forgery noise in high-frequency domains, three convolution kernels aligned with the high-frequency orientations are employed as Eq. 1.

$$hh^e = \{hh', Conv_{xy}(ll')\}, hl^e = \{hl', Conv_x(ll')\}, lh^e = \{lh', Conv_y(ll')\}, \quad (1)$$

where  $hh', hl', lh'$  represent the outputs of the DSConv module, which comprises a  $3 \times 3$  depth-wise convolution followed by a  $1 \times 1$  point-wise convolution.  $ll'$  is the output of WTConv, and  $\{.,.\}$  denotes the concatenate operation.  $Conv_x, Conv_y$ , and  $Conv_{xy}$  are the 2D convolution kernels to extract horizontal, vertical, and diagonal features. Then,  $hh^e, hl^e$ , and  $lh^e$  are concatenated together and processed by a feed-forward network to obtain the wavelet-enhanced feature  $F^e \in R^{3C \times \frac{H}{2} \times \frac{W}{2}}$ . After that, the concatenated features of  $F^e$  and  $ll$  are fed into the inverse wavelet transform, and the resulting output is added to  $I$  to obtain wavelet-enhanced input  $I^e \in R^{C \times H \times W}$ .

To better explore local artifact cues, a Central Correlation Convolution [29] is adopted, which can amplify the local detailed features. Specifically, Central Correlation Convolution consists of two steps. In each convolution, for every pixel, the central pixel value is first subtracted, followed by convolution with the corresponding coefficients. The entire process can be simplified as the subtraction of two convolution operations for computational efficiency, as shown in Eq. 2.

$$\begin{aligned} y(p_0) &= \sum_{p_i \in R^l} w(p_i) * (x(p_{0+i}) - x(p_0)) \\ &= \sum_{p_i \in R^l} w(p_i) * x(p_{0+i}) - x(p_0) * \sum_{p_i \in R^l} w(p_i), \end{aligned} \quad (2)$$

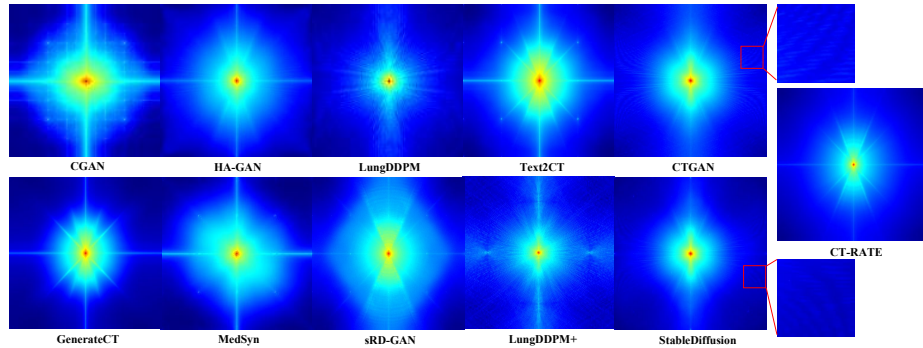


Fig. 3. Frequency Analysis of CTForensics Dataset.

where,  $R^l$  represents the local neighborhood central pixel  $p_0$ , and  $w(\cdot)$  is the parameters of the convolution kernel. Finally, the initial feature map  $F^i$  is then obtained through Batch Normalization, ReLU activation, and MaxPooling operations in sequence.

### 5.3 Spatial Process Block

The Spatial Process Block is used to refine the spatial representation, suppress noise interference in local regions, and aggregate hierarchical features. It consists of two cascaded blocks, where each block processes the input features through successive convolution, Batch Normalization, and ReLU activation functions. In the first block, the stride of the convolution is set to 2 to match the size of the feature map at the next scale, achieving alignment of multi-scale features. Meanwhile, residual connections are incorporated into each block to alleviate the gradient vanishing problem.

### 5.4 Frequency Process Block

As shown in Fig. 3, we visualize the frequency analysis maps of images generated by each generative model and real images, where the frequency map for each category is obtained by averaging the spectral information of multiple images in that category. It can be observed that AI-generated images exhibit significant artifacts in the frequency spectrum, which inspires us to further improve the model’s ability through frequency-domain feature processing. Inspired by previous frequency-based methods [13,29], we directly insert the Fast Fourier Convolution (FFC) [2] into the residual block [8]. The entire process of each Frequency Process Block (FPB) can be expressed as Eq. 3.

$$\hat{F}^f = \phi \circ G \circ \phi \circ N \circ \phi_f(F^f) + F^f, \quad (3)$$

where,  $F^f$  and  $\hat{F}^f$  represent the input and output of FPB, respectively.  $\phi$  is the standard convolution operation, while  $\phi_f$  is the FFC,  $N$  denotes the layer

**Table 1. Accuracy comparison on the CTForensics dataset (%).** The best-performing results are **bolded**.

Methods	CGAN	CTGAN	sRD-GAN	GenerateCT	LungDDPM	LungDDPM+	MedSyn	HA-GAN	StableDiffusion	Text2CT	mAcc
ResNet-50 [8]	51.50	50.00	63.76	50.00	50.00	57.80	<b>100.00</b>	99.98	50.00	50.05	62.31
SAFE [14]	67.00	54.13	62.81	50.00	50.13	50.30	97.13	99.98	59.49	50.15	64.11
UFD [20]	99.88	50.00	51.09	50.00	83.72	70.35	99.15	99.75	49.91	50.32	70.42
NPR [26]	51.88	73.09	53.13	50.00	<b>100.00</b>	82.85	92.83	99.95	78.39	50.08	73.22
FerretNet [16]	67.15	76.94	50.55	51.60	<b>100.00</b>	98.65	96.63	<b>100.00</b>	96.98	50.20	78.87
Freqnet [25]	51.95	<b>98.46</b>	99.86	91.12	79.17	<b>100.00</b>	53.55	99.95	<b>97.93</b>	93.08	86.51
Ours	<b>99.20</b>	89.83	<b>100.00</b>	<b>99.95</b>	<b>100.00</b>	<b>100.00</b>	80.75	<b>100.00</b>	91.12	<b>99.22</b>	<b>96.01</b>

**Table 2. Average precision comparison on the CTForensics dataset (%).** The best-performing results are **bolded**.

Methods	CGAN	CTGAN	sRD-GAN	GenerateCT	LungDDPM	LungDDPM+	MedSyn	HA-GAN	StableDiffusion	Text2CT	mAP
ResNet-50 [8]	97.28	33.67	96.84	39.04	87.62	78.96	<b>100.00</b>	<b>100.00</b>	33.51	47.24	71.42
SAFE [14]	99.95	91.28	89.63	34.60	99.23	87.51	99.99	<b>100.00</b>	94.30	68.50	86.50
UFD [20]	<b>100.00</b>	50.12	84.81	73.56	99.76	98.60	99.98	<b>100.00</b>	66.79	74.58	84.82
NPR [26]	98.98	98.47	91.01	93.37	<b>100.00</b>	99.96	99.99	<b>100.00</b>	99.09	83.58	96.45
FerretNet [16]	99.72	99.05	80.52	98.96	<b>100.00</b>	99.99	<b>100.00</b>	<b>100.00</b>	99.76	80.95	95.90
Freqnet [25]	97.34	<b>99.97</b>	<b>100.00</b>	98.20	99.51	<b>100.00</b>	94.27	<b>100.00</b>	<b>99.97</b>	99.65	98.89
Ours	<b>100.00</b>	99.81	<b>100.00</b>	<b>100.00</b>	<b>100.00</b>	<b>100.00</b>	99.91	<b>100.00</b>	99.89	<b>99.99</b>	<b>99.96</b>

**Table 3. Ablation of used scales.**

Scales	mAcc	mAP
224 <sup>2</sup>	90.43	99.78
224 <sup>2</sup> & 112 <sup>2</sup>	90.86	99.32
224 <sup>2</sup> & 448 <sup>2</sup>	93.28	99.07
<b>224<sup>2</sup> &amp; 112<sup>2</sup> &amp; 448<sup>2</sup></b>	<b>96.01</b>	<b>99.96</b>

**Table 4. Ablation of WEC Stem.**

Wavelet	Central	mAcc	mAP
×	×	88.37	95.24
×	✓	92.03	99.91
✓	×	89.46	97.93
<b>✓</b>	<b>✓</b>	<b>96.01</b>	<b>99.96</b>

normalization, and  $G$  is a Simple Gated Mechanism. Finally,  $\hat{F}^f$  is aggregated by the average pooling, followed by an MLP layer to predict the authenticity. Additionally, binary entropy loss is employed as the loss function.

## 6 Experiments

### 6.1 Implementation Details

We choose Adam as the optimizer with the learning rate of  $2 \times 10^{-4}$ , and adopt CosineAnnealingLR as the learning rate scheduler to dynamically adjust the learning rate during training. Three different image scales are set as follows:  $112 \times 112$ ,  $224 \times 224$ , and  $448 \times 448$ . The batch size is set to 32, and all experiments are conducted on a single NVIDIA RTX 3090 GPU. During training, Horizontal Flip, Gaussian blur and JPEG compression are employed for data augmentation. We adopt Average Precision (AP) and classification Accuracy (Acc) as evaluation metrics, where a threshold of 0.5 is used for Acc.

### 6.2 Performance

**Main Results.** As shown in Tab. 1 and 2, we report the mAP and mAcc on the CTForensics dataset. Our proposed ESF-CTFD achieves 96.01% mAcc and

**Table 5. Performance of CTForensics dataset under various perturbations.**

w/Blur	w/Cropping	w/JPEG	w/Noise	mAcc (ours)	mAcc (Freqnet)	mAcc (FerretNet)	mAcc(NPR)
✓	×	×	×	<b>95.96</b>	75.93	64.63	62.55
×	✓	×	×	<b>94.74</b>	84.29	73.48	69.72
×	×	✓	×	<b>95.99</b>	86.24	72.13	70.89
×	×	×	✓	<b>93.39</b>	84.94	67.41	66.51
✓	✓	✓	✓	<b>95.01</b>	82.95	69.29	67.10
<b>Average Drop</b>				↓ <b>0.99</b>	↓ 3.64	↓ 9.48	↓ 5.87

99.96% mAP, significantly outperforming all the methods. Notably, in terms of mAcc, ESF-CTFD surpasses all existing methods by more than 10%. This demonstrates the superiority of our proposed ESF-CTFD for CT forensics. Moreover, some methods achieve excellent performance in natural image scenarios but degrade significantly on medical images, such as SAFE. This mainly results from the domain gap between natural and medical images, including differences in imaging mechanisms and statistical distributions.

**Ablation Study.** As shown in Tab. 3, multi-scale modeling significantly improves detection performance. Introducing additional resolutions consistently enhances results, and the combination of three scales ( $112\times 112$ ,  $224\times 224$  and  $448\times 448$ ) achieves the best mAcc and mAP, indicating strong cross-scale complementarity in capturing both global structural inconsistencies and subtle local artifacts. Tab. 4 further demonstrates that both the wavelet and central branches in the WEC Stem contribute positively to performance, with the central branch showing a more pronounced effect. Notably, their combination yields a substantial improvement over either branch alone, validating the synergistic integration of spatial correlation modeling and wavelet-aware enhancement.

**Robust Analysis.** As shown in Tab. 5, four various perturbations are applied: (1) Gaussian blurring with kernel size randomly selected from  $\{3, 5, 7, 9\}$ ; (2) random spatial cropping where the cropping ratio is sampled from uniform distribution  $U(5, 20)$  and the cropped region is upsampled to the original resolution; (3) JPEG compression with quality factor sampled from  $U(10, 75)$ ; (4) injection of i.i.d. Gaussian noise with variance sampled from  $U(5.0, 20.0)$ . Notably, even under the combination of all perturbations, the performance remains stable, indicating a high tolerance to diverse input distortions. Averaged over the five perturbation settings, our method exhibits only a 0.99% performance drop, which is substantially lower than that of the competing methods. Its robustness comes from joint modeling of spatial, frequency and multi-scale properties, preserving key forgery cues under degradation.

## 7 Conclusion

In this paper, we introduce CTForensics, a comprehensive dataset for evaluating the generalization of CT forgery detection methods across diverse generative models, which includes ten representative generative approaches and a total of 75,990 images. We also propose ESF-CTFD, an efficient detector that integrates

wavelet, spatial, and frequency-domain cues to capture CT-specific forgery artifacts. Extensive experiments demonstrate that ESF-CTFD consistently outperforms existing methods and exhibits strong generalization and robustness under realistic and perturbed clinical settings.

## References

1. Albahli, S., Nawaz, M.: Mednet: Medical deepfakes detection using an improved deep learning approach. *Multimedia Tools and Applications* **83**(16), 48357–48375 (2024)
2. Chi, L., Jiang, B., Mu, Y.: Fast fourier convolution. In: *Neural Information Processing Systems* (2020)
3. Finder, S.E., Amoyal, R., Treister, E., Freifeld, O.: Wavelet convolutions for large receptive fields. In: *European Conference on Computer Vision*. pp. 363–380. Springer (2024)
4. Goodfellow, I.J., Pouget-Abadie, J., Mirza, M., Xu, B., Warde-Farley, D., Ozair, S., Courville, A., Bengio, Y.: Generative adversarial nets. *Advances in neural information processing systems* **27** (2014)
5. Grabovski, F.M., Yasur, L., Amit, G., Mirsky, Y.: Back-in-time diffusion: Unsupervised detection of medical deepfakes. *ACM Transactions on Intelligent Systems and Technology* **16**(6), 1–26 (2025)
6. Hamamci, I.E., Er, S., Sekuboyina, A., Simsar, E., Tezcan, A., Simsek, A.G., Esirgun, S.N., Almas, F., Doğan, I., Dasdelen, M.F., et al.: Generatect: Text-conditional generation of 3d chest ct volumes. In: *European Conference on Computer Vision*. pp. 126–143. Springer (2024)
7. Hamamci, I.E., Er, S., Wang, C., Almas, F., Simsek, A.G., Esirgun, S.N., Doğan, I., Durugol, O.F., Hou, B., Shit, S., et al.: Developing generalist foundation models from a multimodal dataset for 3d computed tomography. *arXiv preprint arXiv:2403.17834* (2024)
8. He, K., Zhang, X., Ren, S., Sun, J.: Deep residual learning for image recognition. In: *Proceedings of the IEEE conference on computer vision and pattern recognition*. pp. 770–778 (2016)
9. Jiang, Y., Lemaréchal, Y., Bafaro, J., Abi-Rjeile, J., Joubert, P., Després, P., Manem, V.: Lung-ddpm: Semantic layout-guided diffusion models for thoracic ct image synthesis. *arXiv preprint arXiv:2502.15204* (2025)
10. Jiang, Y., Shariftabrizi, A., Manem, V.S.: Lung-ddpm+: Efficient thoracic ct image synthesis using diffusion probabilistic model. *Computers in biology and medicine* **199**, 111290 (2025)
11. Konz, N., Chen, Y., Dong, H., Mazurowski, M.A.: Anatomically-controllable medical image generation with segmentation-guided diffusion models. In: *International Conference on Medical Image Computing and Computer-Assisted Intervention*. pp. 88–98. Springer (2024)
12. Lee, K.W., Chin, R.K.Y.: Diverse covid-19 ct image-to-image translation with stacked residual dropout. *Bioengineering* **9**(11), 698 (2022)
13. Li, J., Xie, H., Li, J., Wang, Z., Zhang, Y.: Frequency-aware discriminative feature learning supervised by single-center loss for face forgery detection. In: *Proceedings of the IEEE/CVF conference on computer vision and pattern recognition*. pp. 6458–6467 (2021)

14. Li, O., Cai, J., Hao, Y., Jiang, X., Hu, Y., Feng, F.: Improving synthetic image detection towards generalization: An image transformation perspective. In: Proceedings of the 31st ACM SIGKDD Conference on Knowledge Discovery and Data Mining V. 1. pp. 2405–2414 (2025)
15. Li, S., Xing, Z., Wang, H., Hao, P., Li, X., Liu, Z., Zhu, L.: Toward medical deepfake detection: A comprehensive dataset and novel method. In: International Conference on Medical Image Computing and Computer-Assisted Intervention. pp. 626–637. Springer (2025)
16. Liang, S., Liu, J., Renzhang, C., Guan, Q.: Ferretnet: Efficient synthetic image detection via local pixel dependencies. In: The Thirty-ninth Annual Conference on Neural Information Processing Systems (2025)
17. Loey, M., Manogaran, G., Khalifa, N.E.M.: A deep transfer learning model with classical data augmentation and cgan to detect covid-19 from chest ct radiography digital images. *Neural computing and applications* **37**(35), 29099–29111 (2025)
18. Mirsky, Y., Mahler, T., Shelef, I., Elovici, Y.: {CT-GAN}: Malicious tampering of 3d medical imagery using deep learning. In: 28th USENIX Security Symposium (USENIX Security 19). pp. 461–478 (2019)
19. Molino, D., Caruso, C.M., Ruffini, F., Soda, P., Guarrasi, V.: Text-to-ct generation via 3d latent diffusion model with contrastive vision-language pretraining. *arXiv preprint arXiv:2506.00633* (2025)
20. Ojha, U., Li, Y., Lee, Y.J.: Towards universal fake image detectors that generalize across generative models. In: Proceedings of the IEEE/CVF Conference on Computer Vision and Pattern Recognition. pp. 24480–24489 (2023)
21. Prezja, F., Paloneva, J., Pölönen, I., Niinimäki, E., Äyrämö, S.: Deepfake knee osteoarthritis x-rays from generative adversarial neural networks deceive medical experts and offer augmentation potential to automatic classification. *Scientific Reports* **12**(1), 18573 (2022)
22. Rombach, R., Blattmann, A., Lorenz, D., Esser, P., Ommer, B.: High-resolution image synthesis with latent diffusion models. In: Proceedings of the IEEE/CVF conference on computer vision and pattern recognition. pp. 10684–10695 (2022)
23. Song, Y., Sohl-Dickstein, J., Kingma, D.P., Kumar, A., Ermon, S., Poole, B.: Score-based generative modeling through stochastic differential equations. *arXiv preprint arXiv:2011.13456* (2020)
24. Sun, L., Chen, J., Xu, Y., Gong, M., Yu, K., Batmanghelich, K.: Hierarchical amortized gan for 3d high resolution medical image synthesis. *IEEE journal of biomedical and health informatics* **26**(8), 3966–3975 (2022)
25. Tan, C., Zhao, Y., Wei, S., Gu, G., Liu, P., Wei, Y.: Frequency-aware deepfake detection: Improving generalizability through frequency space domain learning. In: Proceedings of the AAAI Conference on Artificial Intelligence. vol. 38, pp. 5052–5060 (2024)
26. Tan, C., Zhao, Y., Wei, S., Gu, G., Liu, P., Wei, Y.: Rethinking the up-sampling operations in cnn-based generative network for generalizable deepfake detection. In: Proceedings of the IEEE/CVF Conference on Computer Vision and Pattern Recognition. pp. 28130–28139 (2024)
27. Tan, M., Le, Q.: Efficientnetv2: Smaller models and faster training. In: International conference on machine learning. pp. 10096–10106. PMLR (2021)
28. Xu, Y., Sun, L., Peng, W., Jia, S., Morrison, K., Perer, A., Zandifar, A., Visweswaran, S., Eslami, M., Batmanghelich, K.: Medsyn: text-guided anatomy-aware synthesis of high-fidelity 3-d ct images. *IEEE Transactions on Medical Imaging* **43**(10), 3648–3660 (2024)

29. Yu, Z., Zhao, C., Wang, Z., Qin, Y., Su, Z., Li, X., Zhou, F., Zhao, G.: Searching central difference convolutional networks for face anti-spoofing. In: Proceedings of the IEEE/CVF conference on computer vision and pattern recognition. pp. 5295–5305 (2020)
30. Zhang, T., Liu, P., Lu, Y., Cai, M., Zhang, Z., Zhang, Z., Zhou, Q.: Cwnet: Causal wavelet network for low-light image enhancement. In: Proceedings of the IEEE/CVF International Conference on Computer Vision. pp. 8789–8799 (2025)